Heritage Science

RESEARCH

Open Access

Carbon quantum dots as a tracer of water seepage sources and pathways in grottoes

Bo Sun[1,2,3*], Fenyan Ma[4], Huyuan Zhang[1], Ningbo Peng[5] and Peng Zhang[3]

Abstract

Water seepage is one of the main factors leading to the damage of grottoes. The sources and pathways of water seepage need to be identified to relieve it. Although the sources and pathways are investigated using geophysical exploration methods commonly, the results are unsatisfactory due to the limitation of resolution. The tracer method has been widely used to examine water seepage in the natural sciences and engineering. However, most tracers have an impact on grottoes, making this method inapplicable. This study was the first to use the carbon quantum dots as a tracer of water seepage in grottoes. The characteristics of the carbon quantum dots, which was synthesized by various biomass precursors through large-scale synthesis in the field, were analyzed to determine the optimal precursor. The structure, fluorescence intensity, and water solubility of the carbon quantum dots were evaluated. Laboratory tests were designed to examine the transport properties of the carbon quantum dots in rocks and cracks. The results showed that the carbon quantum dots synthesized by Ginkgo biloba were small and had uniform size, excellent fluorescence, good water solubility and transport ability. Furthermore, the carbon quantum dots were successfully used to tracing the source of water seepage at the chest of the Leshan Giant Buddha. The low cost of synthesis, wide precursors, easy and convenient synthesis methods, friendliness to grottoes, and excellent performance of the carbon quantum dots as a tracer suggest the efficacy of this method. These findings could lead to the widespread use of tracer method in studies of water seepage in grottoes.

Keywords Water seepage, Grottoes, Carbon quantum dots, Trace method

Introduction

Grotto is an important part of human cultural heritage, with a long history, art, science, and technology value. They are valuable resources for understanding the cultural process of human civilization and historical evolution [1]. Most grottoes in China are built on mountains, such as the Leshan Giant Buddha (LGB) and Longmen, Yungang, and Maiji Mountain Grottoes. Long-term weathering and human activities result in damage to grottoes. Water seepage is a significant issue that not only threatens the appearance of grottoes but also affects their main structure. Damage from water seepage has been observed in the JinDeng Temple, Yungang Grottoes, and LGB, besides, spalling and peeling of frescoes was noted in the Mogao Grottoes [2–4].

Water seepage can be relieved by identifying the water source or blocking the pathways between the water source and grottoes [5–7]. Therefore, identifying the sources and pathways is necessary to relieve the issue of water seepage. Grottoes are fragile and must not be damaged during the research process; therefore, most

*Correspondence:
Bo Sun
xbysunbo@163.com
[1] College of Civil Engineering and Mechanics, Lanzhou University, Lanzhou 730000, China
[2] Department of Civil Engineering, Lanzhou University of Technology, Lanzhou 730050, China
[3] Heritage conservation center, Northwest Research Institute Limited Company of China Railway Engineering Corporation, Lanzhou 730000, China
[4] College of Energy and Power Engineering, Lanzhou University of Technology, Lanzhou 730050, China
[5] Faculty of Architecture and Civil Engineering, Huaiyin Institute of Technology, Huai'an 223003, China

methods, which are used in natural sciences and engineering for studying water seepage are restricted or prohibited in grottoes.

Geophysical exploration methods commonly used in the study of water seepage analyses in grottoes include ground-penetrating radar, electrical detection, acoustic exploration, ground nuclear magnetic resonance, and infrared thermography [8, 9]. Most water seepage pathways in grottoes are located in mountains and are deep underground. The nondestructive detection of seepage pathways through geophysical exploration methods is affected by resolution, making it difficult to accurately detect seepage pathways and resulting in unsatisfactory results regarding water seepage in grottoes [10, 11]. Besides, monitoring of seepage water volume and water content in rocks and soils, to understand their response to precipitation could summarize the distribution characteristics of water seepage damage, developmental patterns, and spatial and temporal variations [12, 13]. It provides a basis for investigating the source of water seepage, but it is difficult to identify the source and pathways of water seepage. Therefore, modifying existing geophysical exploration methods and identifying new methods to research the sources and pathways of water seepage in grottoes is important.

The tracer method is widely used in natural science and engineering to examine the sources and pathways of water seepage. It mainly involves putting tracers, such as dyes, fluorescents, salts, and isotopes, in the suspected seepage location and detecting the tracers at the water seepage point and seepage pathways [14, 15]. This method is a direct and effective method to identify the sources and pathways of water seepage. Scholars have studied the source of water in the cliffs of the Mogao Grottoes through the tracer method with stable isotopes. It was found that water vapour from phreatic water evaporation transports to the cliffs and becomes one of the main reasons for the peeling off of wall paintings in the Mogao Grottoes [16]. Hydrogen and oxygen, as the constituent elements of water, have strong advantages as tracer, but the measurement cost is expensive [17, 18]. Besides, δ^2H and $\delta^{18}O$ are changed due to evaporation during the seepage process, which will be errors in the process of identifying the source of water seepage, and other methods are needed to further support the results [19]. The sources of water seepage could be determined more accurately by artificial tracers, however, it is rarely used in grottoes, as most tracers are damaging. Identifying a non-destructive tracer for grottoes is a priority.

The unique physical and chemical properties of fluorescent nanoparticles have led to widespread interest in sensing and imaging analyses. Additionally, the efficacy of nanomaterials as tracers and their transportability in porous media due to their good water solubility have been demonstrated [20–22]. For instance, nanomaterials have been successfully applied to characterize oil reservoirs and trace groundwater flows in porous media [4, 23, 24].

Carbon quantum dots (CQDs) are new fluorescent nanoparticles with low cytotoxicity, good biocompatibility, excellent fluorescence, various synthesis methods, and ease of detection. CQDs is an excellent alternative to traditional fluorescent nanomaterials and are widely used in the fields of pharmaceuticals, biology, food, medicine, and the environment [25, 26]. Although studies on using CQDs as water seepage tracer are scarce, CQDs is superior to traditional nanomaterials owing to their excellent fluorescence, good water solubility, low cytotoxicity, and environmental friendliness [27]. Additionally, the use of CQDs as a tracer of water seepage in grottoes is promising because of their nondamaging nature.

The characteristics of the CQDs depend on precursor, synthesis method, solvent type, and synthesis time [28]. Different synthesis methods and precursors result in different water solubilities and fluorescence of the CQDs. This study aimed to identify an effective precursor with large-scare synthesis method and evaluate the feasibility of using the CQDs obtained with this method to trace the sources and pathways of water seepage in grottoes. This study examined the source of water seepage from the chest of the LGB using the CQDs as a tracer.

Materials and methods

Materials of the CQDs synthesis

This study used 1300 g of fresh Ginkgo biloba, Osmanthus flowers, Osmanthus leaves, Willow leaves, and Sequoia leaves as precursors, respectively. The precursors were washed three times with deionized water (DI water), then placed in a 15 L pressure cooker with 13 L of DI water and heated for 3 h (Fig. 1). The mixture was then cooled to room temperature. The liquid portion of the mixture was isolated by filtration, followed by centrifugation at 12,000 rpm for 10 min to remove smaller impurities. The resulting supernatant containing fluorescent CQDs was dialyzed against DI water for two days to remove all inorganic ions and molecules and obtain a pure CQDs solution, which was subsequently characterized. The fluorescence quantum yield, particle characteristics, and minimum detectable concentration of the CQDs synthesized from the different precursors were subsequently analyzed, and the optimal precursor was selected for further analysis.

Measurement of the CQDs

Transmission electron microscopy (TEM) and selected area electron diffraction (SAED) images were acquired

Fig. 1 Diagram of the CQDs synthesis

using JEM-2100 F TEM operating (JEOL, Japan) at an acceleration voltage of 200 kV. X-ray diffraction (XRD) of the CQDs was performed using D/Max-2400 X-ray diffractometer (Rigaku, Japan) with Cu Kα radiation. Fourier-transform infrared (FTIR) spectroscopy was conducted using Thermo Nicolet Nexus FTIR Model 670 spectrometer (Thermo Fisher Scientific, USA). X-ray photoelectron spectroscopy (XPS) was performed using ESCALAB 250xi photoelectron spectrometer (Thermo Fisher Scientific, USA). PL measurements were conducted using FLS 1000 steady state/transient state spectroxsort (Edinburgh Instruments, UK).

The Photoluminescence Quantum Yield (PLQY) of the CQDs, which refers to the efficiency of light emission from the CQDs upon excitation was calculated using the following equation [29]:

$$\phi = \phi'\left(\frac{m}{m'}\right)\left(\frac{\eta}{\eta'}\right)^2$$

where ϕ and ϕ' are the PLQY of the sample and standard, respectively; sample and standard are the slopes of the plot of integrated fluorescence intensity vs. absorbance; and sample and standard are the refractive indices of the solvent.

Laboratory tracer tests

The rock samples, which were used in the laboratory tracer tests were from a quarry around the LGB and sedimentary rock, which was the same material as the LGB (Fig. 2). The rock samples are cylinders with a height and diameter of 25 cm and 8 cm respectively. Six tests were conducted to compare the fluorescence changes of the

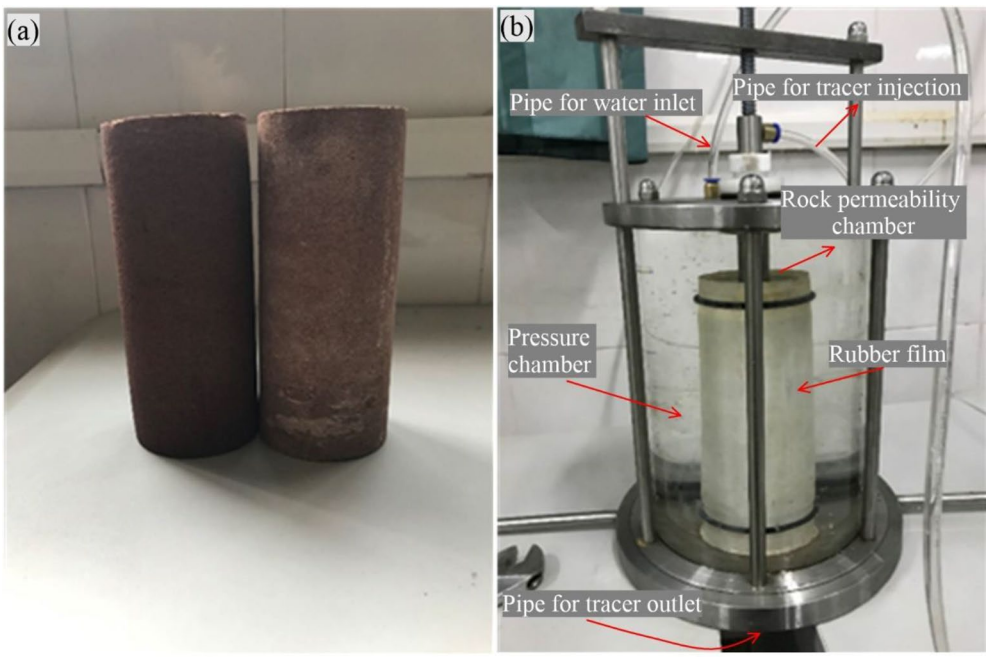

Fig. 2 The rock samples used in the laboratory tracer tests (**a**) and the test device for laboratory tracer tests (**b**)

solution after passing rock sample with different concentrations of the CQDs solutions (ratios of the original CQDs solution to DI water: 1:50, 1:100, 1:200, 1:300, 1:400, and 1:500) and assess the transport properties of the CQDs.

The laboratory tracer tests were carried out in a self-developed test device, which mainly consists of a pressure chamber, rock permeability chamber, pipes for tracer injection and outlet, and a pipe for water inlet (Fig. 2). The rock sample was placed into the rock penetration chamber, which is separated from the pressure chamber by rubber film. Prior to the test, DI water was flowed into the pressure chamber through the pipe for water inlet and the water head of the pressure chamber was higher than that of the rock permeability chamber to ensure that the tracer can't flow out of the rock sample from the side during the test process. The CQDs solution was injected into rock permeability chamber through the pipe for tracer injection, while the seepage solution was collected from pipes for tracer outlet. The fluorescence of the CQDs solutions injected and collected from pipes for tracer outlet were compared and analyzed. Additionally, to prevent the solution of the previous test from remaining inside the rock sample and affecting its detection accuracy in the next test, the rock sample was rinsed with DI water after every test to minimize errors. The rinsing process involves the continuous injection of DI water, with a volume of 1 L, into the rock sample through the pipe for tracer injection.

Tracer test for water seepage of LGB

The solution, obtained by mixing the original solution of the CQDs with water (1:1), was injected into the water accumulation point on Lingyun Mountain, the foot of which was built into the LGB. Water seepage samples were collected continuously from the cracks in the chest of the LGB (collection times were 1, 52, 54, 56, 58, and 60 h after injection of the CQDs solution). High-density polyethylene bottles (100 ml) were used for sampling. After sampling was completed, the samples were sealed and brought back to the laboratory to measure fluorescence. The test was permitted by Leshan Giant Buddha Grotto Research Institute.

Results and discussion

CQDs synthesized by different precursors

Before using CQDs to trace water seepage in grottoes, it is necessary to pre-rear them on a large scale in field and maintain similar physical properties. CQDs can be synthesized by various precursors, and their yields and morphologies vary significantly based on precursors; therefore, the selection of a suitable precursor is a prerequisite for the large-scale use of CQDs as a tracer [30, 31]. CQDs synthesized by green precursors have significant potential for tracing water seepage in grottoes owing to their low cytotoxicity [32, 33].

A high yield and fluorescence of the CQDs significantly reduces costs and detection difficulty, respectively. Meanwhile, a uniform distribution and small size result in stronger transport of the CQDs [34]. When the CQDs are transported with groundwater, the CQDs solution will be diluted due to mixing with other water. Therefore, minimal detectable concentration is a key to tracing water seepage using CQDs. To identify suitable precursors, a lot of natural green plants (leaves or flowers) were sampled to synthesize the CQDs. The CQDs synthesized using green plants had different yields, morphologies, and minimum detectable concentrations. Most green plants cannot synthesize CQDs in large quantities. Five green plants were selected, and the synthesized CQDs were analyzed in detail.

The yields, size characteristics, fluorescence quantum yields, and minimum detectable concentrations of the CQDs solutions synthesized from the five precursors (Ginkgo biloba leaves, Osmanthus cinnamomi flowers, Osmanthus cinnamomi leaves, Willow leaves, and Metasequoia leaves) are listed in Table 1. The highest yield of the CQDs was synthesized from Ginkgo biloba, followed by Osmanthus flowers, Osmanthus leaves, Willow leaves, and Metasequoia leaves.

The CQDs synthesized from willow leaves had no obvious granularity, whereas those from the other precursors had uniform particles and smaller average

Table 1 Characteristics of the CQDs synthesized from various precursors

Characteristics	Ginkgo biloba leaves	Osmanthus flowers	Osmanthus leaves	Willow leaves	Metasequoia leaves
CQDs yields	40 mg/500 g	1.5 mg/500 g	2.5 mg/500 g	6 mg/500 g	4 mg/500 g
Size distribution	2–6 nm	2–8 nm	2–9 nm	Unobvious granularity	2–7 nm
Mean size	3.1 nm	4.4 nm	4.3 nm	Unobvious granularity	3.6 nm
Fluorescence quantum yields	6.2%	0.9%	1.3%	0.6%	1.1%
Minimum detectable concentrations	2.0 ng/L	220 ng/L	170 ng/L	180 ng/L	150 ng/L

size. Ginkgo biloba leaves had the most uniform particle (70% of the CQDs were distributed between 3 and 4 nm) and smallest average size (Fig. 3). The fluorescence quantum yield of Ginkgo biloba leaves exceeded that of Osmanthus flowers, and Osmanthus, Willow, and Metasequoia leaves. The minimum detectable concentration of the CQDs synthesized from Ginkgo biloba leaves was approximately 1/100 of that of Osmanthus flowers, and Osmanthus, Willow, Metasequoia leaves. As such, the CQDs synthesized from Ginkgo biloba leaves had the highest yield, uniform particle size, smallest size, highest fluorescence quantum yield, and lowest detectable concentration. Additionally, the CQDs were synthesized in an autoclave, which allowed synthesis in large quantities in the field. This method saved considerable labor and material resources compared to the hydrothermal synthesis method, which requires large energy consumption in the laboratory. Furthermore, the ubiquity of the precursors in nature greatly enhances the feasibility of using the CQDs as a tracer for studying water seepage in grottoes.

Characterization of CQDs

Unharmful to grottoes is a prerequisite for tracing water seepage; however, most tracers, such as NaCl, KI and fluorescent dyes, are colored or likely to crystallize in seepage pathways [14]. Crystallization of the tracer in the seepage pathways may lead to the formation of new cracks, resulting in more severe seepage pathways; thus, the tracer method has not been widely used in the water seepage of grottoes [35]. Good water solubility and amorphous of the tracer during the tracing process are the basis for examining water seepage in grottoes.

The TEM image revealed that the CQDs were spherical and well dispersed in water (Fig. 3). No distinct lattice fringes appeared in the SAED image, indicating that the CQDs had an amorphous structure, which was consistent with the XRD results (Fig. 3). The XRD pattern exhibited one broad diffraction peak at $2\theta = 20.8°$, which could be attributed to amorphous carbon [36]. The amorphous structure prevented crystallization in cracks that occurs with KI, which is a widely used tracer. Therefore, the ultrasmall size and amorphous structure of the

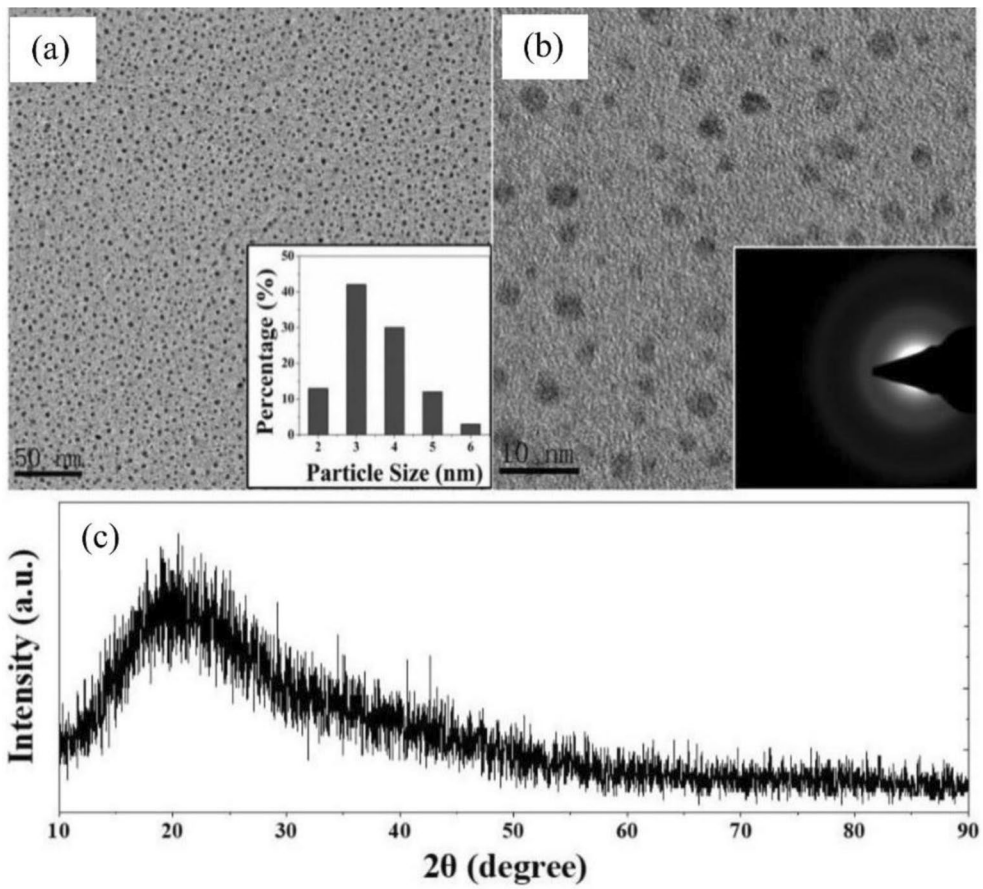

Fig. 3 TEM and HRTEM image of the CQDs (**a**, **b**) and XRD pattern of the CQDs (**c**)

CQDs suggest their potential application in water seepage studies.

Water solubility is another important indicator for tracer to study water seepage. FTIR spectroscopy and XPS were used to identify the functional groups in the CQDs. As shown in Fig. 4a, the CQDs exhibited a main characteristic absorption band of O–H stretching vibration mode at 3374.9 cm^{-1}, whereas a C-H stretching vibration band appeared at 2931.3 cm^{-1}, and the band at 1658.5 cm^{-1} corresponded to C=C stretching vibration band. The small vibration band at 1716.4 cm^{-1} was attributed to the carbonyl (C=O) groups. Three weak peaks at 1523.5, 1079.9, and 1033.7 cm^{-1} were assigned to N-H, C-O-C, and C-O functional groups, respectively [37]. XPS was used to characterize the functional groups on the surface of the CQDs. A wide XPS survey scan was conducted, and the results are shown in Fig. 4b. The results indicated that the CQDs mainly contained carbon and oxygen, with a small amount of nitrogen. The C:O:N atomic ratio calculated from the XPS spectrum was 40.4:15.4:2.2. As shown in Fig. 4c, the C1s feature was deconvoluted into five unit moieties: C-C with a binding energy at 282.6 eV, C–N at 285.9 eV, C=C at 284.2 eV, C–O at 285.2 eV, and C=O at 286.5 eV. The O1s feature (Fig. 4d) was deconvoluted into peaks at 529.1, 530.7, and 530.0 eV, corresponding to C-O, C=O, and C-O groups, respectively [38]. FTIR spectroscopy and XPS results indicated the presence of a significant density of carboxylic acid and hydroxyl groups in the CQDs, implying that the CQDs should be stable against aggregation and settling in water. Furthermore, the good dispersion of the CQDs, as shown in the TEM images, suggested good water solubility.

The fluorescence properties of the CQDs are critical as a tracer. To investigate the fluorescence properties of the CQDs, a detailed PL study was conducted at different excitation wavelengths. In these measurements, the emission peaks shifted from 433.6 to 553.6 nm with an increase in excitation wavelength from 300 to 500 nm (Fig. 5a). The unique excitation-dependent PL behavior is beneficial for water seepage tracing, as it allows CQDs to be easily identified in the natural environment, especially when separated from materials with PL performance. To account for possible dilution by natural sources of water, such as precipitation, PL spectra of the CQDs solutions of different concentrations were measured. As shown in Fig. 5b, the

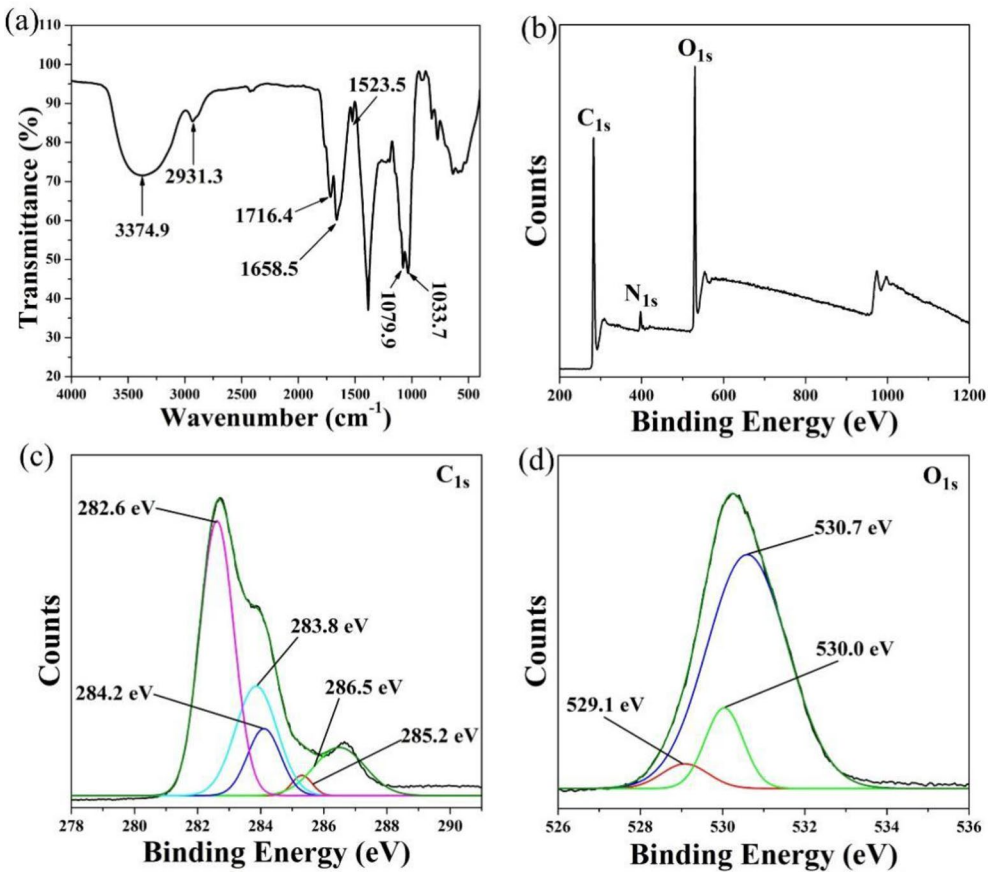

Fig. 4 **a** FTIR spectrum of the CQDs; **b** wide XPS survey spectrum of the CQDs; **c** C_{1s} detailed spectrum; **d** O_{1s} detailed spectrum of the CQDs

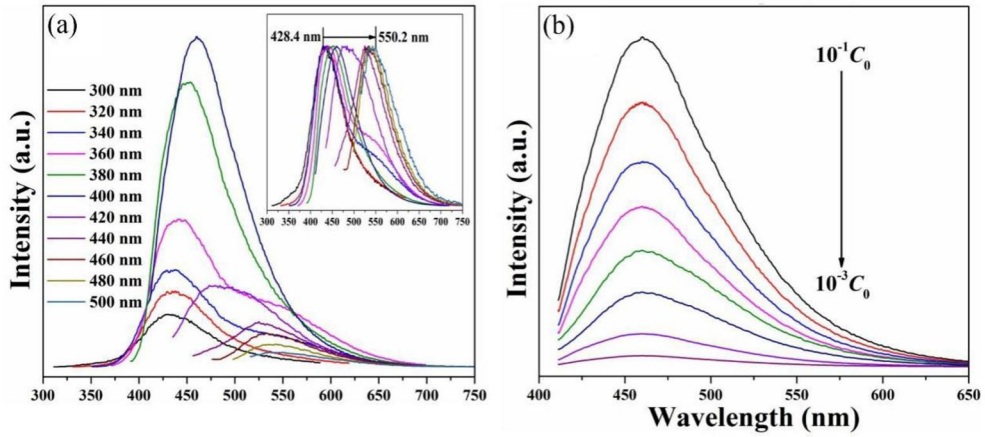

Fig. 5 **a** PL spectra of CQDs with excitation wavelengths ranging from 300 to 500 nm, inset: normalized PL spectra, **b** PL spectra of CQDs with concentrations ranging from 10^{-1} C_0 to 10^{-3} C_0, λ_{ex} = 400 nm

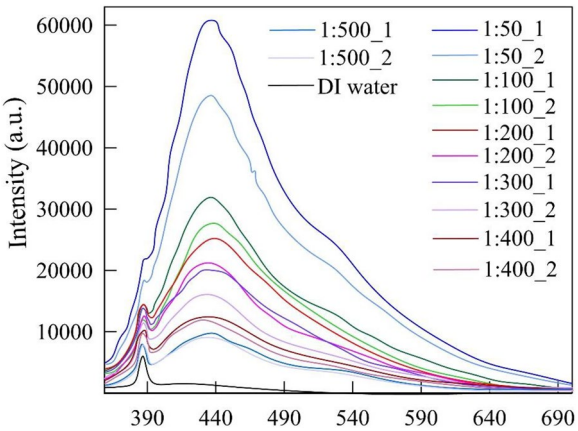

Fig. 6 Fluorescence intensity of the CQDs solutions of various concentration before and after flowing through rock sample

PL signal was detected even when the CQDs solution was attenuated 1000 times. The calculated PLQY of the CQDs solution was as high as 6.2% (details in CQDs synthesized by different precursors), which was comparable to that of previously reported CQDs [39]. In summary, CQDs can be used as a tracer to examine water seepage in grottoes.

Ability of CQDs to flow with water

To evaluate the ability of the CQDs to trace water seepage in grottoes, it is important to examine their ability to flow with water through rocks and cracks [40]. The fluorescence of the CQDs solution decayed after injection into the rock samples. However, the degree differed with different concentrations of the CQDs (Fig. 6). Due to the similarity of the results of the laboratory tracer tests through the two rock samples, only the tracer results of one rock sample are analyzed in the paper.

The solution, when mixed with the original CQDs solution in a 1:50 ratio of water, exhibited higher fluorescence intensity compared to the other solutions. However, the fluorescence intensity decayed significantly (20%) after flowing through the rock sample. Among the six tests, the solution with a 1:300 ratio of the original CQDs solution to water flowed through the rock sample with the highest fluorescence decay of 23%. The fluorescence intensity of the solutions, which are formed from the original CQDs solution and water in ratios of 1:100, 1:200, 1:400, and 1:500 decay is lower than 15% after flowing through the rock sample and were 12%, 13%, 7%, and 9%, respectively.

There were two main reasons for the decay in the fluorescence of the CQDs solution after flowing out of a rock sample. As the rock sample were rinsed with DI water before each test, a lot of DI water was preserved in the rock, and the CQDs solution, injected into the rock sample mixed with the DI water in the rock sample, resulting in dilution of the CQDs solution, which led to fluorescence intensity decay. In addition, all fluorescent tracers have a hysteresis in the process of flowing with water, and the CQDs did not completely flows out of the rock sample while gravitational water flows out completely during the tracing process, resulting in fluorescence intensity decay. The rock sample was treated in the same manner before every test and was the same in all tests. It was hypothesized that the dilution of the CQDs solution with water in the rock sample was the same. Furthermore, the small amount of water in the rock sample had less of an effect on the dilution of the highly concentrated CQDs solutions. Therefore, the difference in the decay of the different concentrations of the CQDs solutions after flowing through the rock sample was mainly due to the difference in the amount of CQDs retained in the rock sample.

The six tests indicated that most of the CQDs flowed out of the rock sample with the water. Although some CQDs were retained in the rock sample, their quantity was small, relative to the total CQDs. The CQDs were amorphous and did not widen the cracks or form new cracks in the rock. Moreover, owing to good water solubility, the CQDs retained in the seepage pathways flowed out under prolonged water flow after tracer tests in field. Therefore, CQDs were shown to be excellent tracers of the sources and pathways of water seepage in grottoes.

CQDs transport properties for LGB

The LGB is the largest stone of the Maitreya Buddha sitting statue and is over one thousand years old. Owing to long-term weathering, LGB has suffered a variety of damage, with water seepage cited as the primary cause. Cracks were found on the chest of the LGB, and there was evident water seepage that seriously threatened the longevity of the LGB (Fig. 7). Finding the source of water seepage in the chest of the LGB is a top priority for solving water seepage.

As the CQDs has an ultrasmall size, amorphous structure, good water solubility, and PL performance, it is a good choice for tracing in grottoes. The synthesis method which was shown in this study, produced low-cost with high productivity. To further examine the performance of the CQDs as a tracer, a test was conducted on the LGB using the CQDs solution to trace the source of water seepage. The PL spectrum was detected at the chest of the LGB with excitation wavelengths of 320 and 400 nm.

Significant fluorescence was detected in all the water samples collected from the chest of the LGB after the CQDs were injected into the water accumulation point on Lingyun Mountain. There was a weak fluorescence in the water samples 1 h after the injection of the CQDs, and the fluorescence was the highest at 52 h. After this, the fluorescence gradually weakened and was weaker at 60 h than at 1 h (Fig. 8). Tracing test showed that the water in Lingyun Mountain was the source of water seepage from the chest of the Big Buddha. During the whole

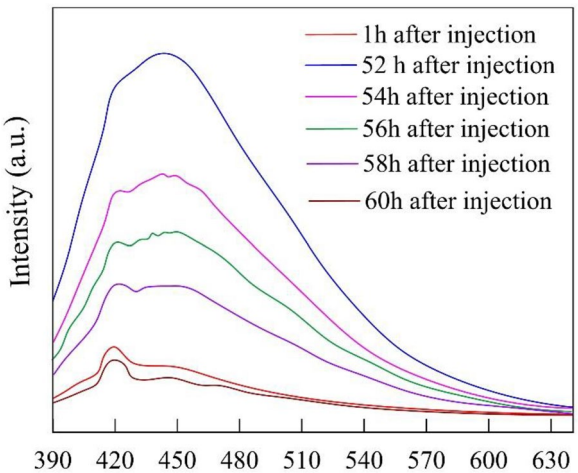

Fig. 8 Fluorescence intensity in the water samples collected from the cracks of the LGB's chest after the CQDs solutions were injected into the water accumulation point on Lingyun Mountain

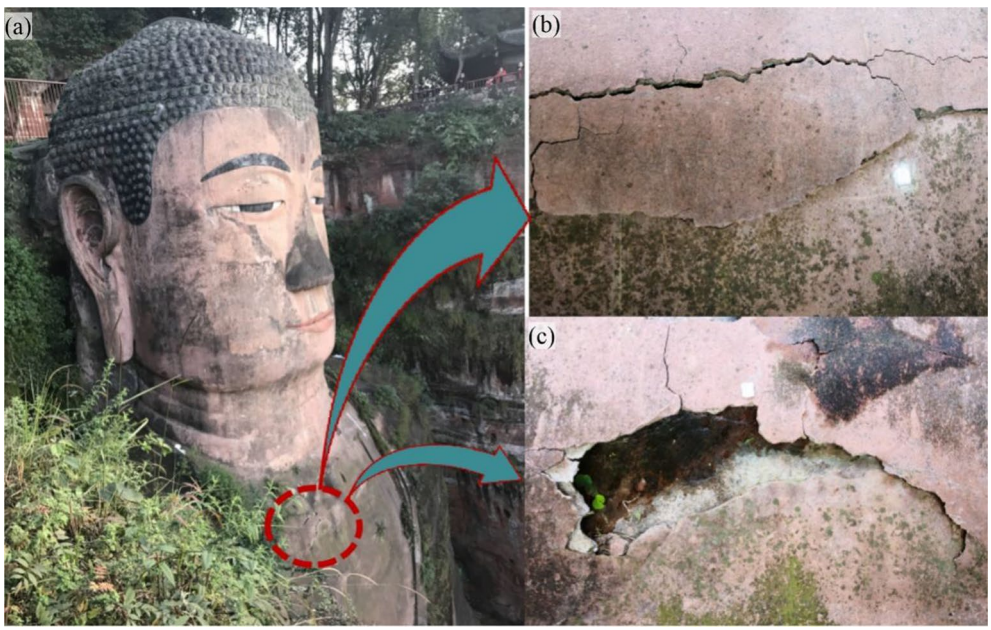

Fig. 7 **a** Photos of LGB; **b** and **c** the cracks on the chest of the LGB

test period, the fastest rate of fluorescence intensity weakening was observed between 52 and 54 h, suggesting that most of the CQDs flowed out of the water seepage pathways in this period.

The weak fluorescence intensity of the water samples at 60 h indicated that most of the CQDs already flowed out. Therefore, the transport time for the water from the area where the CQDs were injected to the cracks at the chest of the LGB was less than 60 h, and the transport time of water flowing in the cracks was between 52 and 54 h. The results of tracer tests on LGB demonstrated that the CQDs are good tracers of sources and pathways of water seepage in grottoes owing to their high accuracy, low cost, safety, and reliability.

Conclusions

In this study, the CQDs was considered as a tracer to study the sources and pathways of water seepage in grottoes. An effective precursor with large-scare synthesis method was selected and the characterization of obtained CQDs was analyzed. In addition, laboratory tracer tests were carried out to understand the transport properties of the CQDs and it was used to identify the sources of water seepage in the chest of the LGB. The results demonstrated that the synthesis, characterization, and testing of the CQDs provide the foundation for their future use as a tracer of water seepage in grottoes.

The CQDs synthesized from Ginkgo biloba leaves had smaller and uniform particles, amorphous structure with high fluorescence quantum yield, minimum detectable concentrations and good water solubility. Laboratory tests revealed that the fluorescence of the CQDs solutions of various concentrations decayed after flowing through rock sample; however, the degree of decay was low, indicating that the CQDs had a strong transportation ability in water flow. These characteristics ensured that the CQDs could flow out of the seepage pathways with water, and the small amount remaining in the pathways would not crystallize and damage grottoes. The successful injection of the CQDs solution into the precipitation accumulation point on Lingyun Mountain and the detection of the fluorescence characteristics of the water in the chest demonstrated that the accumulation point on the mountain was one source of water seepage in the chest. The transportation time of water from the accumulation point to the chest of the LGB was determined to be less than 60 h based on the fluorescence of the seepage water collected at different times.

The results of this study indicated that the CQDs are an excellent tracer of water seepage in grottoes. Moreover, all steps, including tracer synthesis, seepage detection, and analysis, could be conducted in the field if miniaturized PL equipment is used, greatly improving efficiency and reducing costs. Because the PL emission peak of the CQDs is not obvious, the concentration of the CQDs cannot be obtained, so that the water velocity only estimated through the variation of fluorescence intensity of the CQDs with time the rather than the tracer dilution theory. It is necessary to search for a more suitable precursor in the next study, and improve the suitability of the CQDs as a tracer to make it more suitable for tracing the water seepage in the grottoes. Currently, the CQDs have some limitations, but it opens a new horizon for the tracer method to be widely used to trace water seepage and provide new ideas for the study of water seepage in grottoes.

Abbreviations

LGB	Leshan Giant Buddha
CQDs	Carbon quantum dots
DI water	Deionized water
TEM	Transmission electron microscopy
SAED	Selected area electron diffraction
XRD	X-ray diffraction
FTIR	Fourier-transform infrared
XPS	X-ray photoelectron spectroscopy

Acknowledgements

The authors gratefully acknowledge Mr. Xueyi Peng and Tianyu Yang (Leshan Buddha management committee) are thanked for their kind support.

Author contributions

BS and FM carried out all the analyses and drafted the manuscript. HZ participated in the design on the study. NP analyzed the patient data. PZ performed tracer experiments in the field. All authors read and approved the final manuscript.

Funding

This research was funded by National Natural Science Foundation of China (21603002, 51808246), Natural Science Foundation of Anhui Province (1908085QE221).

Data availability

The datasets used and/or analyzed during the current study are available from the corresponding author on reasonable request.

Declarations

Ethics approval and consent to participate

Ethics approval was not required for this research.

Consent for publication

All authors have consented to publication.

Competing interests

The authors declare no competing interests.

Received: 1 August 2023 Accepted: 20 September 2023
Published online: 02 October 2023

References

1. Fu L, Ding MJ, Zhang QP. Flood risk assessment of urban cultural heritage based on PSR conceptual model with game theory and cloud model-a case study of Nanjing. J Cult Herit. 2022;58:1–11.

2. Wang J. Visualizing water seepage dynamics in grotto relics via atom-based representative model. Herit Sci. 2023;11(1):1.
3. Liu BL, Peng WY, Li HD, Qu JJ. Increase of moisture content in Mogao Grottoes from artificial sources based on numerical simulations. J Cult Herit. 2020;45:135–41.
4. Jones EH, Smith CC. Non-equilibrium partitioning tracer transport in porous media: 2-D physical modelling and imaging using a partitioning fluorescent dye. Water Res. 2005;39(20):5099–111.
5. Qin YW, Qiu JL, Lai JX, Liu FY, Wang LX, Luo YB, Liu T. Seepage characteristics in loess strata subjected to single point water supply. J Hydrol. 2022;609:127611.
6. Rosenberry DO, Morin RH. Use of an electromagnetic seepage meter to investigate temporal variability in lake seepage. Ground Water. 2004;42(1):68.
7. Davidson GR, Rigby JR, Pennington D, Cizdziel JV. Elemental chemistry of sand-boil discharge used to trace variable pathways of seepage beneath levees during the 2011 Mississippi River flood. Appl Geochem. 2013;28:62–8.
8. Li H, Ma HT. Application of ground penetrating radar in dam body detection. Ismsse. 2011;2011(26).
9. Huang SQ. Leakage detection methods for reservoir dams. Dam and Safety. 2021;2:42–50.
10. Zhao Y, Zeng ZF, Li J, Zhou S, Lu P, Huo ZJ. Application status and prospect of geophysical detection technology in fracture seepage of grottoes. Prog Geophys. 2022;37(2):0928–37.
11. Day-Lewis FD, Slater LD, Robinson J, Johnson CD, Terry N, Werkema D. An overview of geophysical technologies appropriate for characterization and monitoring at fractured-rock sites. J Environ Manage. 2017;204:709–20.
12. Yuan W, Kan Y, Zeng K. Analysis on causes of water damage in Pilu Cave Grottoes in Anyue. Groundwater. 2022;44(03):45–7.
13. Sun B, Zhang H, Zhang P, Shen X, Yang T. Study on the characteristics of seepage disease in the chest-abdomen of Leshan Giant Buddha. J Southwest Jiaotong Univ. 2022.
14. Cheng JS, Li XW, Zhao WB. Study on piping leakage mechanism. J Hydraul Eng. 2000;09:48–54.
15. Liu JG, Cheng JS, Chen L, Yang ST. Study of seepage in low-dip bedded structure of Xiaolangdi Dam abutment by tracer method. Chin J Rock Mechan Eng. 2004;23(8):1339–43.
16. Li H, Zhang H, Qiu F. Use of δD and $\delta^{18}O$ to determine the source of evaporation water in Dunhuang Mogao Grottoes. Arid Land Geography. 2017;40(06):1179–87.
17. Ma FY, Chen JQ, Chen JS, Wang T. Environmental drivers of precipitation stable isotopes and moisture sources in the Mongolian Plateau. J Hydrol, 2023. 621:129615
18. Chen JS, Li L, Wang JY, Barry DA, Sheng XF, Gu WZ, Zhao X, Chen L. Water resources: groundwater maintains dune landscape. Nature. 2004;432(7016):459–60.
19. Ma F, Chen J, Zhan L, Wang T, Yan J, Zhang X. Coastal upward discharge of deep basalt groundwater through developed faults: a case study of the Subei Basin, China. J Environ Manage. 2022;306: 114469.
20. Yu C, Guo X, Gao X, Yu Z, Jiang J. Transport of graphene quantum dots (GQDs) in saturated porous media. Colloids Surf A: Physicochemical and Engineering Aspects. 2020. https://doi.org/10.1016/j.colsurfa.2020.124418.
21. Wang YG, Li YS, Fortner J, Hughes D, Abriola JB, Pennell KD. Transport and retention of nanoscale C-60 aggregates in water-saturated porous media. Environ Sci Technol. 2008;42(10):3588–94.
22. Wang C, Bobba AD, Attinti R, Shen C, Lazouskaya V, Wang LP, Jin Y. Retention and transport of silica nanoparticles in saturated porous media: effect of concentration and particle size. Environ Sci Technol. 2012;46(13):7151–8.
23. Hu Z, Gao H, Ramisetti SB, Zhao J, Nourafkan E, Glover PWJ, Wen D. Nanoparticle-assisted water-flooding in Berea Sandstones. Energy Fuels. 2016;30(4):2791–804. https://doi.org/10.1016/j.scitotenv.2019.03.007.
24. Yu H, He Y, Li P, Li S, Zhang T, Rodriguez-Pin E, et al. Flow enhancement of water-based nanoparticle dispersion through microscale sedimentary rocks. Sci Rep. 2015;5: 8702. https://doi.org/10.1038/srep08702.
25. Mao YN, Wang J, Gao YH, Zhao TT, Xu SH, Luo XL. Progress in synthesis and sensing imaging of biomass-based carbon quantum dots. Chin J Anal Chem. 2021;49(7):1076–88.
26. Namdari P, Negahdari B, Eatemadi A. Synthesis, properties and biomedical applications of carbon-based quantum dots: an updated review. Biomed Pharmacother. 2017;87:209–22.
27. Dua S, Kumar P, Pani B, Kaur A, Khanna M, Bhatt G. Stability of carbon quantum dots: a critical review. RSC Adv. 2023;13(20):13845–61. https://doi.org/10.1039/d2ra07180k.
28. Kumar P, Dua S, Kaur R, Kumar M, Bhatt G. A review on advancements in carbon quantum dots and their application in photovoltaics. RSC Adv. 2022;12(11):6432–6432. https://doi.org/10.1039/d2ra90018a.
29. Deng Z, Lie FL, Shen S, Ghosh I, Mansuripur M, Muscat AJ. Water-based route to ligand-selective synthesis of ZnSe and Cd-doped ZnSe quantum dots with tunable ultraviolet A to blue photoluminescence. Langmuir. 2009;25(1):434–42. https://doi.org/10.1021/la802294e.
30. Liu R, Wu D, Feng X, Muellen K. Bottom-Up fabrication of photoluminescent graphene quantum dots with uniform morphology. J Am Chem Soc. 2011;133(39):15221–3. https://doi.org/10.1021/ja204953k.
31. Govarthanan M, Liang Y, Kamala-Kannan S, Kim W. Eco-friendly and sustainable green nano-technologies for the mitigation of emerging environmental pollutants. Chemosphere. 2022. https://doi.org/10.1016/j.chemosphere.2021.132234.
32. Manikandan V, Lee NY. Green synthesis of carbon quantum dots and their environmental applications. Environ Res, 2022. 212(Pt B): p. 113283.
33. Wareing TC, Gentile P, Phan AN. Biomass-based carbon dots: current development and future perspectives. ACS Nano. 2021;15(10):15471–501.
34. Hu Z, Gao H, Ramisetti SB, Zhao J, Nourafkan E, Glover PWJ, Wen D. Carbon quantum dots with tracer-like breakthrough ability for reservoir characterization. Sci Total Environ. 2019;669:579–89.
35. Li X, Chen X, Zhan SB, Wang ZL, Wang XD. Analysis on crystallization procsss and mechanism of limestone fissure water in highway tunnel drainage system. J Highway Transportaion Res Dev. 2023;40(04):136–42.
36. Peng J, Gao W, Gupta BK, Liu Z, Romero-Aburto R, Ge L, et al. Graphene quantum dots derived from carbon fibers. Nano Lett. 2012;12(2):844–9. https://doi.org/10.1021/nl2038979.
37. Arumugam N, Kim J. Synthesis of carbon quantum dots from broccoli and their ability to detect silver ions. Mater Lett. 2018;219:37–40.
38. Wei J, Zhou B, Gu S, Lv S, Zhou Y, Liu B. Facile synthesis of fluorescent carbon nanodots from cornstalk and their application as a sensing platform for detection of Cu2 + ions. Sci Adv Mater. 2017;9(6):901–6. https://doi.org/10.1166/sam.2017.3064.
39. Baker SN, Baker GA. Luminescent Carbon Nanodots: Emergent Nanolights. Angewandte Chemie-International Edition. 2010;49(38):6726–44.
40. Warsi T, Bhattacharjee L, Thangamani S, Jat SK, Mohanta K, Bhattacharjee RR, Ramaswamy R, Manikyamba C, Rao TV. Emergence of robust carbon quantum dots as nano-tracer for groundwater studies☆. Diam Relat Mater. 2020;103:107701.

Publisher's Note